From linear to nonlinear parametric structural dynamics

Giacomo Quaranta, [a] Clara Argerich Martin, [b] Ruben Ibañez, [c] Emmanuelle Abisset, [c] Jean Louis Duval, [a] Elias Cueto, [d] Francisco Chinesta [c]

[a] *ESI GROUP*
99, rue des Solets, 94513 Rungis CEDEX, France.
[b] *GeM Ecole Centrale de Nantes*
1, rue de la Noe, 44321 Nantes Cedex 3, France.
[c] *ESI GROUP Chair @ ENSAM ParisTech*
151 Boulevard de l'Hôpital, F-75013 Paris, France.
[d] *Aragon Institute of Engineering Research, Universidad de Zaragoza*
Edificio Betancourt. Maria de Luna, s.n., 50018, Zaragoza, Spain

Received *****; accepted after revision +++++

Abstract

The present paper analyzes different integration schemes of solid dynamics in the frequency domain. In some of our former works [Advanced parametric space-frequency separated representations in structural dynamics: A harmonic-modal hybrid approach. M.H. Malik, D. Borzacchiello, J.V. Aguado, F. Chinesta, COMPTES RENDUS MECANIQUE 346 (7), 590-602, 2018] we considered such a formulation within the PGD framework. It assumes for the solution a parametric dependency with respect to frequency. This procedure allowed introducing other parametric dependences related to loading, geometry and material properties. However, in these cases affine decompositions are required for an efficient computation of separated representations. A possibility for circumventing such difficulty consists in combining modal and harmonic analysis for defining an hybrid integration scheme. Moreover, such a procedure, as proved in the present work, can be easily generalized to address nonlinear parametric dynamics, as well as to solve problems with non-symmetric stiffness matrices.

Key words: Linear and nonlinear parametric dynamics; Proper Generalized Decomposition; Harmonic analysis; Modal analysis

Email addresses: giacomo.quaranta@ec-nantes.fr (Giacomo Quaranta,), clara.argerich-martin@ec-nantes.fr (Clara Argerich Martin,), Ruben.Ibanez-Pinillo@eleves.ec-nantes.f (Ruben Ibañez,), emmanuelle.abisset-chavanne@ec-nantes.fr (Emmanuelle Abisset,), Jean-Louis.Duval@esi-group.com (Jean Louis Duval,), ecueto@unizar.es (Elias Cueto,), Francisco.Chinesta@ensam.eu (Francisco Chinesta).

1. Introduction

Governing equations in solid dynamics are usually formulated either in the time or in the frequency domains. The former is preferred when calculating transient responses, whereas the frequency approach is an appealing choice for calculating forced responses. Both approaches have been extensively used and described in many classical books as, for instance [10].

Time descriptions are used in both the linear and the nonlinear cases, being specially efficient when combined with modal analysis. This allows expressing the solution on a series of decoupled ordinary differential equations. Other works considered advanced space-time separated representations of transient dynamics [3,5,15]. Recently, a PGD-based dynamical integrator that takes as parameter the field of initial boundary conditions—conveniently expressed in a reduced basis—has also been developed [14,12].

As discussed in [11,13,16], problems become a bit more complex in the case of parametrized dynamics, and more concretely when those parameters depend on frequency. In this case, frequency-based modeling seems more appropriate than its time counterpart, as soon as the functional forms expressing the parametric dependence on frequency are compatible with the use of a space-frequency-parameters separated representation [7,9,1,8].

We review in this introduction, for completeness, the case of linear dynamics and the harmonic-modal hybrid approach developed in [17].

1.1. *Classical linear dynamics in the time or frequency domains*

The general, semi-discretized form of the linear solid dynamics equations writes

$$\mathbf{M}\frac{d^2\mathbf{U}(t)}{dt^2} + \mathbf{C}\frac{d\mathbf{U}(t)}{dt} + \mathbf{K}\mathbf{U}(t) = \mathbf{F}(t), \tag{1}$$

where $\mathbf{M}$, $\mathbf{C}$ and $\mathbf{K}$ are respectively the mass, damping and stiffness matrices. $\mathbf{U}$ represents the vector that contains the nodal displacements and $\mathbf{F}$ the nodal excitations (forces). This equation can be obtained through any suitable mesh-based discretization technique like, for instance, the Finite Element Method.

By moving to the frequency-domain through the Fourier transform $\mathcal{F}(\bullet)$—denoting $\hat{\mathbf{F}}(\omega) = \mathcal{F}(\mathbf{F}(t))$ and $\hat{\mathbf{U}}(\omega) = \mathcal{F}(\mathbf{U}(t))$—, it results

$$\left(-\omega^2\mathbf{M} + \mathrm{i}\omega\mathbf{C} + \mathbf{K}\right)\hat{\mathbf{U}}(\omega) = \hat{\mathbf{F}}(\omega). \tag{2}$$

If damping vanishes, i.e., $\mathbf{C} = \mathbf{0}$ (if it is not the case, it can be assumed to be proportional, $\mathbf{C} = a_0\mathbf{M} + a_1\mathbf{K}$), and one focuses on the free response of the system, $\hat{\mathbf{F}}(\omega) = \mathbf{0}$, Eq. (2) reduces to:

$$\mathbf{K}\hat{\mathbf{U}} = \omega^2\mathbf{M}\hat{\mathbf{U}}. \tag{3}$$

This defines an eigenproblem whose result is given by the eigenmodes $\mathbf{P}_i$ and the associated eigenfrequencies ω_i^2. The inverse transform allows coming back to the time domain, $\mathbf{U}(t) = \mathcal{F}^{-1}(\hat{\mathbf{U}}(\omega))$.

1.2. *A hybrid harmonic-modal approach*

When damping is neglected $\mathbf{C} = \mathbf{0}$ (or when proportional damping is considered $\mathbf{C} = a_0\mathbf{M} + a_1\mathbf{K}$) the single-parameter (frequency) dynamic equation reads

$$\left(-\omega^2\mathbf{M} + \mathbf{K}\right)\hat{\mathbf{U}}(\omega) = \hat{\mathbf{F}}(\omega). \tag{4}$$

We now consider matrix $\mathbf{P}$ diagonalizing matrices $\mathbf{M}$ and $\mathbf{K}$. In other words,

$$\begin{cases} \mathbf{P}^T\mathbf{M}\mathbf{P} = \mathbb{M} \\ \mathbf{P}^T\mathbf{K}\mathbf{P} = \mathbb{K} \end{cases},$$

where $\mathbb{M}_{ij} = m_{ii}\delta_{ij}$ and $\mathbb{K}_{ij} = k_{ii}\delta_{ij}$. Here, δ_{ij} represents the Kroenecker's delta, i.e., $\mathbb{M}$ and $\mathbb{K}$ become diagonal with entries m_{ii} and k_{ii}, respectively.

Such a choice implies that the system is no longer described in terms of its nodal degrees of freedom but rather in terms of the modal content. Both are formally related through the linear transformation

$$\hat{\mathbf{U}}(\omega) = \mathbf{P}\boldsymbol{\xi}(\omega). \tag{5}$$

Thus, the dynamical problem reduces to [17]

$$\left(-\omega^2\mathbb{M} + \mathbb{K}\right)\boldsymbol{\xi}(\omega) = \mathbf{P}^T\hat{\mathbf{F}}(\omega) = \hat{\mathbf{f}}(\omega), \tag{6}$$

that results in a system of N_n decoupled algebraic equations (N_n being the size of matrices $\mathbf{M}$ and $\mathbf{K}$)

$$\left(-\omega^2 m_{ii} + k_{ii}\right)\xi_i(\omega) = \hat{f}_i(\omega), \quad i = 1, 2, \ldots, N_n, \tag{7}$$

from which it results

$$\xi_i(\omega) = \frac{\hat{f}_i(\omega)}{(-\omega^2 m_{ii} + k_{ii})}, \quad i = 1, 2, \ldots, N_n, \tag{8}$$

that allows calculating the nodal amplitudes from Eq. (5), i.e. $\hat{\mathbf{U}}(\omega) = \mathbf{P}\boldsymbol{\xi}(\omega)$.

Thus, the space-frequency separated representation reads

$$\hat{\mathbf{U}}(\omega) = \sum_{i=1}^{N_n} \mathbf{Z}_i\xi_i(\omega), \tag{9}$$

where $\mathbf{Z}_i$ is the i-column of matrix $\mathbf{P}$.

The obtention of $\hat{\mathbf{U}}(\omega)$ allows us to come back to the time domain $\mathbf{U}(t)$ by applying an inverse Fourier transform,

$$\mathbf{U}(t) = \mathcal{F}^{-1}(\hat{\mathbf{U}}(\omega)).$$

It is important to highlight—this will be crucial later when addressing nonlinear dynamics—that each term $\xi_i(\omega)$ involves transformed nodal forces, that is, nodal forces affected by the transformation matrix $\mathbf{P}$. Thus, Eq. (9) represents a canonical space-frequency-loading separated representation, that only makes use of a proportional damping assumption.

1.3. *Extension to dynamics involving non-symmetric stiffness matrices*

Above, matrices $\mathbf{M}$ and $\mathbf{K}$ were considered symmetric, making us possible to diagonalize them according to Eq. (13). Some dynamical systems, which will be discussed later, like networks composed of Helmholtz resonators, lead to non-symmetric stiffness matrices $\mathbf{K}_{\text{NS}}$. The rationale considered above can be extended accordingly by just defining the symmetric matrix $\mathbf{K}_{\text{S}}$ such that

$$\mathbf{K}_{\text{S}} = \mathbf{K}_{\text{NS}} + \mathbf{K}_{\text{NS}}^T, \tag{10}$$

and rewriting the dynamical system according to

$$\mathbf{M}\frac{d^2\mathbf{U}(t)}{dt^2} + \left(\mathbf{K}_{\text{NS}} + \mathbf{K}_{\text{NS}}^T - \mathbf{K}_{\text{NS}}^T\right)\mathbf{U}(t) = \mathbf{F}(t), \tag{11}$$

or, equivalently,

$$\mathbf{M}\frac{d^2\mathbf{U}(t)}{dt^2} + \mathbf{K}_{\mathrm{S}}\mathbf{U}(t) = \mathbf{F}(t) + \mathbf{K}_{\mathrm{NS}}^T\mathbf{U}(t). \tag{12}$$

Thus, the left-hand side of the previous equation can be diagonalized according to

$$\begin{cases} \mathbf{P}^T\mathbf{M}\mathbf{P} = \mathbb{M} \\ \mathbf{P}^T\mathbf{K}_S\mathbf{P} = \mathbb{K} \end{cases}, \tag{13}$$

that leads to

$$\left(-\omega^2\mathbb{M} + \mathbb{K}\right)\boldsymbol{\xi}(\omega) = \mathbf{P}^T\hat{\mathbf{F}}(\omega) = \hat{\mathbf{f}}(\omega), \tag{14}$$

where, in the present case, $\hat{\mathbf{F}}(\omega)$ is the Fourier transform of the right-hand side of Eq. (12), i.e.,

$$\hat{\mathbf{F}}(\omega) = \mathcal{F}(\mathbf{F}(t) + \mathbf{K}_{\mathrm{NS}}^T\mathbf{U}(t)). \tag{15}$$

This term will be linearized, in the framework of an iterative scheme, by simply evaluating $\mathbf{U}(t)$ at the previous converged iteration.

The time solution can be obtained by applying the inverse transform to the frequency solution $\hat{\mathbf{U}}(\omega) = \mathbf{P}\boldsymbol{\xi}(\omega)$, according to

$$\mathbf{U}(t) = \mathcal{F}^{-1}(\hat{\mathbf{U}}(\omega)) = \mathcal{F}^{-1}(\mathbf{P}\boldsymbol{\xi}(\omega)).$$

2. Nonlinear dynamics

In the nonlinear case, the general semi-discretized equilibrium equation writes

$$\mathbf{M}\frac{d^2\mathbf{U}(t)}{dt^2} + \mathbf{C}\frac{d\mathbf{U}(t)}{dt} + \mathbf{K}\mathbf{U}(t) - \mathbf{H}(\mathbf{U}) = \mathbf{F}(t),$$

where the nonlinear contribution is grouped in the vector $\mathbf{H}(\mathbf{U})$.

The simplest linearization of this equation consists in an explicit evaluation of the non-linear term $\mathbf{H}(\mathbf{U})$ at the last converged iteration. For the sake of notational simplicity it will be denoted by $\mathbf{U}^-(t)$. Thus, as soon as the nonlinear contribution is assumed known, it can be moved to the right hand member, i.e.,

$$\mathbf{M}\frac{d^2\mathbf{U}(t)}{dt^2} + \mathbf{C}\frac{d\mathbf{U}(t)}{dt} + \mathbf{K}\mathbf{U}(t) = \mathbf{H}(\mathbf{U}^-(t)) + \mathbf{F}(t). \tag{16}$$

An obvious possibility consists in computing the Fourier transform of the right-hand member of Eq. (16),

$$\hat{\mathbf{F}}(\omega) = \mathcal{F}(\mathbf{H}(\mathbf{U}^-(t)) + \mathbf{F}(t)),$$

and then to proceed exactly in the same way as in the linear case. However, in order to take benefit of model order reduction, in what follows we present an alternative but equivalent formulation, more adapted to the use of reduced bases.

By invoking the linearity of Fourier transform, we write

$$\hat{\mathbf{F}}(\omega) = \mathcal{F}\left(\mathbf{H}(\mathbf{U}^-(t)) + \mathbf{F}(t)\right) = \mathcal{F}\left(\mathbf{H}(\mathbf{U}^-(t))\right) + \mathcal{F}\left(\mathbf{F}(t)\right) = \hat{\mathbf{F}}^{\mathrm{H}}(\omega) + \hat{\mathbf{F}}^{\mathrm{F}}(\omega),$$

that could be expressed using a piecewise linear approximation basis $N_l(\omega)$ (like the usually considered one in linear finite element analyses)

$$\hat{\mathbf{F}}^{\mathrm{H}}(\omega) = \sum_{l=1}^{\mathtt{L}} \hat{\mathbf{F}}^{\mathrm{H}}(\omega_l)N_l(\omega),$$

or, equivalently,

$$\hat{\mathbf{F}}^{\mathrm{H}}(\omega) = \mathbf{P}^T \hat{\mathbf{F}}^{\mathrm{H}}(\omega).$$

In turn,

$$\hat{\mathbf{F}}^{\mathrm{F}}(\omega) = \sum_{l=1}^{\mathtt{L}} \hat{\mathbf{F}}^{\mathrm{F}}(\omega_l) N_l(\omega),$$

or

$$\hat{\mathbf{F}}^{\mathrm{F}}(\omega) = \mathbf{P}^T \hat{\mathbf{F}}^{\mathrm{F}}(\omega),$$

each one contributing to the solution $\boldsymbol{\xi}(\omega)$ according to

$$\boldsymbol{\xi}(\omega) = \boldsymbol{\xi}^{\mathrm{H}}(\omega) + \boldsymbol{\xi}^{\mathrm{F}}(\omega), \tag{17}$$

with

$$\xi_i^{\mathrm{H}}(\omega) = \frac{\sum_{l=1}^{\mathtt{L}} \hat{f}_i^{\mathrm{H}}(\omega_l) N_l(\omega)}{(-\omega^2 m_{ii} + k_{ii})}, \qquad i = 1, 2, \cdots, N_n, \tag{18}$$

$$\xi_i^{\mathrm{F}}(\omega) = \frac{\sum_{l=1}^{\mathtt{L}} \hat{f}_i^{\mathrm{F}}(\omega_l) N_l(\omega)}{(-\omega^2 m_{ii} + k_{ii})}, \qquad i = 1, 2, \cdots, N_n. \tag{19}$$

Thus, it finally results

$$\hat{\mathbf{U}}(\omega) = \mathbf{P}\boldsymbol{\xi}(\omega) = \hat{\mathbf{U}}^{\mathrm{H}}(\omega) + \hat{\mathbf{U}}^{F}(\omega) = \mathbf{P}\boldsymbol{\xi}^{\mathrm{H}}(\omega) + \mathbf{P}\boldsymbol{\xi}^{F}(\omega),$$

being its time-dependent counterpart

$$\mathbf{U}(t) = \mathbf{U}^{\mathrm{H}}(t) + \mathbf{U}^{\mathrm{F}}(t) = \mathcal{F}^{-1}(\mathbf{P}\boldsymbol{\xi}^{\mathrm{H}}(\omega)) + \mathcal{F}^{-1}(\mathbf{P}\boldsymbol{\xi}^{\mathrm{F}}(\omega)).$$

It is important to highlight that the inverse transform involves terms $\mathcal{T}_{il}$, $i = 1, \ldots, N_n$ and $l = 1, \ldots, \mathtt{L}$, whose form reads

$$\mathcal{T}_{il} \equiv \mathcal{F}^{-1}\left(\frac{N_l(\omega)}{-\omega^2 m_{ii} + k_{ii}}\right),$$

and that can be computed offline and stored in memory.

Our numerical experiments reveal that this offline-online procedure does not allow for significant computing time savings when one considers a standard piecewise linear approximation bases. However, by considering reduced bases to approximate functions $\hat{\mathbf{F}}^{\mathrm{H}}(\omega)$ and $\hat{\mathbf{F}}^{\mathrm{F}}(\omega)$, the number of integrals to be performed drastically reduces and the offline-online becomes valuable. These reduced basis are computed offline after an adequate training stage. Moreover, the computational cost for the evaluation of the nonlinear term in the time domain, $\mathbf{H}(\mathbf{U}^{-}(t))$, can be drastically reduced by using empirical interpolation techniques [4,6,2].

As soon as reduced bases are available in the frequency domain, their counterpart in the time domain is easily computable, and from it, direct Fourier transform could be also computed offline. The use of strategies based on the use reduced bases constitutes a work in progress.

3. Numerical results

3.1. *Nonlinear dynamics*

In this section we use the proposed strategy to address the 1D dynamics of a rod of length L, cross section A, clamped at its left boundary and subjected to an axial load applied on its right boundary as depicted in Figure 1.

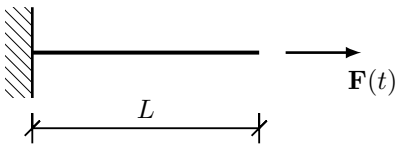

Figure 1. Simple case study.

If a linear elastic behavior is assumed, the relation between the stress σ and the strain ε reads

$$\sigma = E\,\varepsilon,$$

where E is the Young modulus. In every simulation we used $L = 1m$, $E = 2{\cdot}10^9 N/m^2$ and $\rho = 8000kg/m^3$, where ρ is the density. When damping vanishes or when proportional damping is assumed, the mechanical response is computed from the discrete system

$$\mathbf{M}\frac{d^2\mathbf{U}(t)}{dt^2} + \mathbf{K}\mathbf{U}(t) = \mathbf{F}(t), \tag{20}$$

whose expression in the frequency domain is given by Eq. (4). However when a nonlinear elastic behavior is assumed, the stress-strain relation reads

$$\sigma = \mathcal{C}(\varepsilon),$$

where $\mathcal{C}$ is a non-linear function of ε. In the numerical test here addressed it is assumed that

$$\sigma = E\,(\varepsilon + c\,\varepsilon^3), \tag{21}$$

where c can be considered as a parameter (obviously, when $c = 0$ the nonlinear case reduces to the linear case).

Recalling the linearization described in Section 2, the mechanical response is computed from the discrete system

$$\mathbf{M}\frac{d^2\mathbf{U}(t)}{dt^2} + \mathbf{C}\frac{d\mathbf{U}(t)}{dt} + \mathbf{K}\mathbf{U}(t) = c\,\mathbf{H}(t) + \mathbf{F}(t), \tag{22}$$

where $\mathbf{H}(t)$ accounts for the nonlinear contribution.

Thus, using the notation introduced in the previous section, the frequency and time domain solutions read

$$\hat{\mathbf{U}}(\omega; c) = \hat{\mathbf{U}}^{\mathrm{F}}(\omega) + c\hat{\mathbf{U}}^{\mathrm{H}}(\omega), \tag{23}$$

that can be seen as a parametric solution involving both the frequency ω and the parameter c controlling the nonlinearity, with its time counterpart expressed from

$$\mathbf{U}(t, c) = \mathcal{F}^{-1}(\hat{\mathbf{U}}^{\mathrm{F}}(\omega)) + c\mathcal{F}^{-1}(\hat{\mathbf{U}}^{\mathrm{H}}(\omega)). \tag{24}$$

Both formulations, the one defined in the time domain and the harmonic-modal hybrid formulations are solved in the time interval $I = [0, T]$ with $T = 4s$, the first by using a standard Newmark time-stepping (with time step $\Delta t = 10^{-2}s$).

Figure 2 compares both solutions for two different values of the parameter c: $c = 0$ that corresponds to the linear case and for $c = 220$ for the simple harmonic loading $F(t) = 10^{10}\sin(2\pi t)$. The computed results agree perfectly, but when using the hybrid solver significant computing time savings are noticed. These are summarized in Tables 1 and 2. Moreover, Table 1 also reflects the fact that the computing time saving remains almost independent of the considered mesh size.

Finally, we consider a more complex loading scenario, as depicted in Fig. 3. It contains a richer frequency spectrum, with $c = 0$ and $c = 4000$. The solutions when using the Newmark ($\Delta t = 10^{-3}\,s$) versus the harmonic-modal hybrid schemes are again in perfect agreement, as Fig. 4 reveals, with similar computing time savings, reported in Tables 3 and 4.

Table 1
Hybrid vs Newmark methods, $T = 4\,s$.

	Hybrid	Newmark
$N_n = 100$	$1.34\,s$	$5.97\,s$
$N_n = 250$	$3.26\,s$	$14.29\,s$
$N_n = 500$	$7.19\,s$	$39.08\,s$
$N_n = 750$	$11.70\,s$	$68.12\,s$
$N_n = 1000$	$16.33\,s$	$100.75\,s$

Table 2
Fourier vs Newmark method, $N_n = 100$.

	Hybrid	Newmark
$T = 4\,s$:	$1.34\,s$	$5.97\,s$
$T = 8\,s$:	$2.44\,s$	$12.20\,s$
$T = 20\,s$:	$6.32\,s$	$29.75\,s$
$T = 40\,s$:	$13.54\,s$	$59.30\,s$

Table 3
Fourier vs Newmark method, $T = 4\,s$.

	Hybrid	Newmark
$N_n = 100$:	$2.49\,s$	$9.68\,s$
$N_n = 250$:	$6.90\,s$	$23.38\,s$
$N_n = 500$:	$14.28\,s$	$48.26\,s$
$N_n = 750$:	$21.90\,s$	$69.72\,s$
$N_n = 1000$:	$30.13\,s$	$93.11\,s$

Table 4
Fourier vs Newmark method, $N_x = 100$.

	Hybrid	Newmark
$T = 4\,s$:	$2.49\,s$	$9.68\,s$
$T = 8\,s$:	$4.95\,s$	$21.32\,s$
$T = 20\,s$:	$13.57\,s$	$59.48\,s$
$T = 40\,s$:	$28.29\,s$	$122.23\,s$

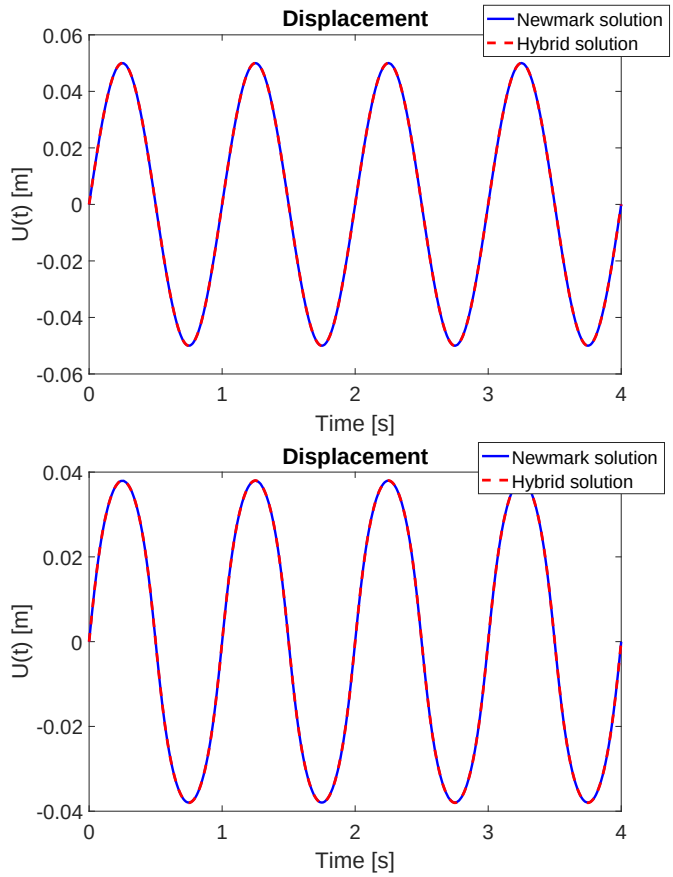

Figure 2. Displacement at the rod right border for two different values of c: (top) $c = 0$, that corresponds to the linear case and (bottom) $c = 220$.

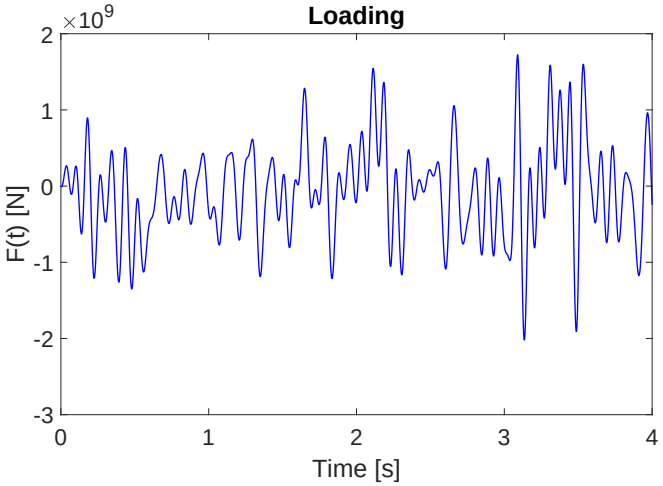

Figure 3. *Loading containing a richer frequency spectrum*

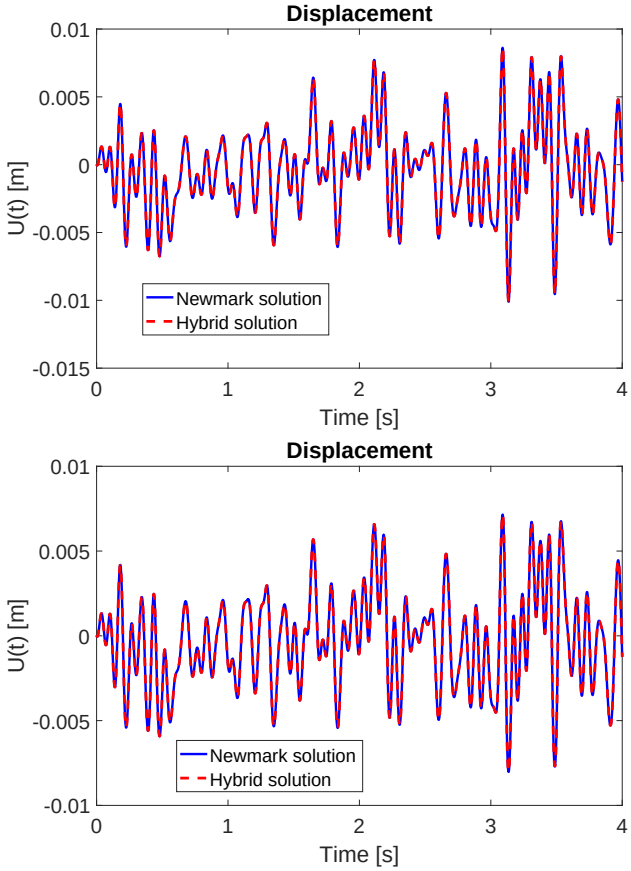

Figure 4. Displacement at the rod right border for two different values of c: (top) $c = 0$, that corresponds to the linear case and (bottom) $c = 4000$.

3.2. *Non-symmetric stiffness*

In this section we consider a network of Helmholtz resonators, depicted in Fig. 5. Here, the oscillation amplitude of the air in each pipe contributes to the compression of the air filling the cavities connecting different tubes. That compression results in a pressure variation that generates an extra force, acting at the entrance section of each tube. In each tube the inertia contribution involves the second time-derivative of the oscillation amplitude. The whole model results in a quite standard dynamical system with the only exception of containing a non-symmetric stiffness matrix. In that case, the modal-harmonic hybrid method is applied as described in Section 2, that proceeds by symmetrizing the problem before applying the hybrid strategy.

As can be noticed from Fig. 5, the geometry of the system follows a fractal structure. Therefore, the geometrical characteristics of subsequent generations will be determined by the characteristics of the first generation: the tube cross section, A_1, the tube length l_1, and the cavity volume, V_1. Subsequent generations are characterized by a given reduction factor, in our case of 2. Standard thermodynamical air properties are considered.

The model of a single Helmholtz resonator reads

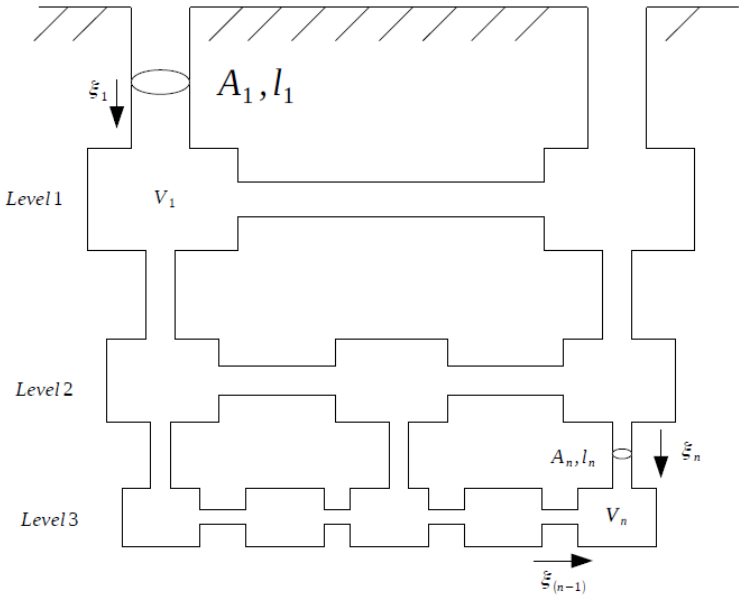

Figure 5. Case of study for non-symmetric dynamics.

$$\rho AL\frac{d^2U(t)}{dt^2} + \frac{\gamma pA^2}{V}U(t) = f(t),$$

and, by assembling the contribution of those involved in the network of Fig. 5, it results

$$\mathbf{M}\frac{d^2\mathbf{U}(t)}{dt^2} + \mathbf{K}\mathbf{U}(t) = \mathbf{F}(t),$$

where

$$\mathbf{M}_{ii} = \rho A_i L_i,$$
$$\mathbf{K}_{ij} = \gamma P_0 A_i A_j \frac{1}{V^{ij}}, \text{ for } i \neq j,$$

with j referring to a tube connected to one of the cavities associated to tube i, with volume V^{ij}, and

$$\mathbf{K}_{ii} = -\gamma P_0 A_i^2 \sum_{j=1}^{N_i} \frac{1}{V^{ij}},$$

where N_i refers to all the tubes connected with the cavities associated to tube i.

The discrete system involves the dynamics of the air displacement in each tube and its only specificity concerns the fact of having a non-symmetric stiffness matrix. Figure 6 compares the solution obtained by using the modal-harmonic hybrid techniques described in Section 2 and the reference solution obtained by a standard time-stepping integration. A perfect agreement between both solutions can be noticed. Figure 7 depicts the convergence of the iteration scheme involved by the use of the hybrid formulation, where error ϵ is defined as

$$\epsilon = \frac{||\mathbf{U}^i(t) - \mathbf{U}^{i-1}(t)||}{||\mathbf{U}^i(t)||},$$

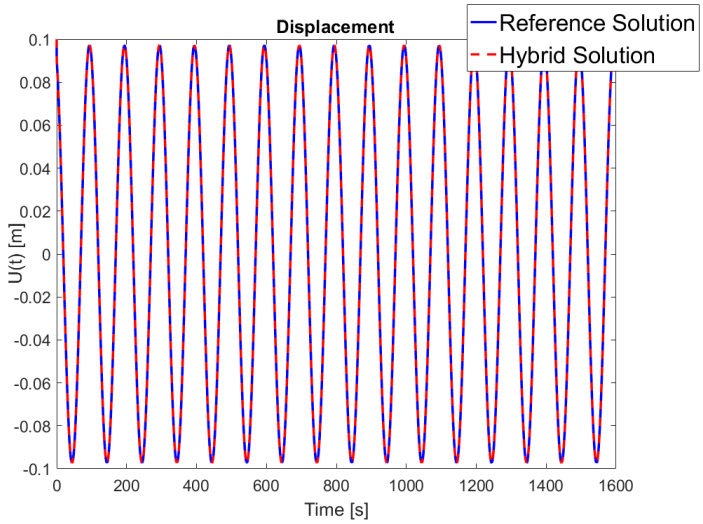

Figure 6. Displacement of the air filling the first tube.

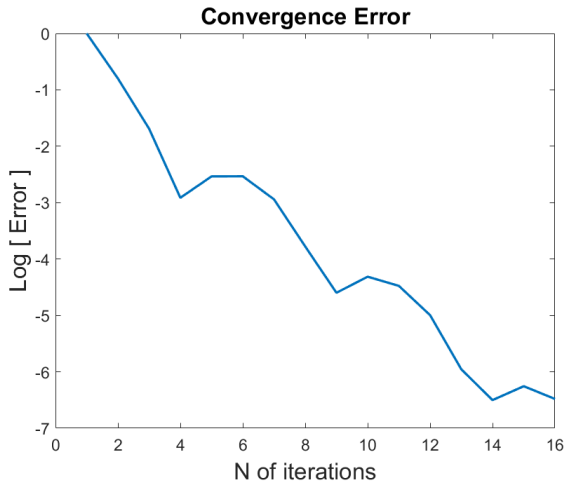

Figure 7. Convergence analysis.

where the i-superscript refers to the iteration within the hybrid strategy. As it can be noticed, convergence is reached very fast.

4. Conclusions

In this note we proposed an extension of the hybrid methodology combining harmonic and modal analyses for treating nonlinear parametric dynamics.

The main contribution of the present work is the derivation of a parametric solution in the frequency space. Apart from its natural dependence on the frequency, the just developed method also accounts for other model parameters. More importantly, it explicitly decouples the dependence on the amplitude

of nodal loading. This last fact makes possible the solution of nonlinear models combined with simple linearizations.

Preliminary numerical results evidence the potentialities of the proposed technique, while proving its computational efficiency.

Acknowledgements

This work has been supported by the Spanish Ministry of Economy and Competitiveness through Grants number DPI2017-85139-C2-1-R and DPI2015-72365-EXP and by the Regional Government of Aragon and the European Social Fund, research group T24 17R. This project has also received funding from the European Union's Horizon 2020 research and innovation programme under the Marie Sklodowska-Curie grant agreement No. 675919.

References

[1] J.V. Aguado, A. Huerta, F. Chinesta and E. Cueto. Real-time monitoring of thermal processes by reduced order modelling. *International Journal for Numerical Methods in Engineering*, 102/5, 991-1017, 2015

[2] J.V. Aguado, D. Borzacchiello, Ch. Ghnatios, F. Lebel, R. Upadhyay, C. Binetruy, F. Chinesta. A Simulation App based on reduced order modeling for manufacturing optimization of composite outlet guide vanes. Adv. Model. and Simul. in Eng. Sci., 4:1 DOI 10.1186/s40323-017-0087-y, 2017.

[3] A. Barbarulo, H. Riou, L. Kovalevsky and P. Ladeveze. PGD-VTCR: A reduced order model technique to solve medium frequency broad band problems on complex acoustical systems. *Journal of Mechanical Engineering*, 60/5, 307-314, 2014.

[4] M Barrault, Y Maday, N.C Nguyen, A.T Patera. An empirical interpolation method: application to efficient reduced-basis discretization of partial differential equations. *Comptes Rendus Mathematique*, 339/9, 667-672, 2004.

[5] L. Boucinha, A. Ammar, A. Gravouil and A. Nouy. Ideal minimal residual-based proper generalized decomposition for non-symmetric multi-field models - Application to transient elastodynamics in space-time domain. *Computer Methods in Applied Mechanics and Engineering*, 273, 56-76, 2014

[6] S. Chaturantabut and D.C. Sorensen. Nonlinear model reduction via discrete empirical interpolation. *SIAM Journal on Scientific Computing* 32(5):2737-2764, 2010.

[7] F. Chinesta, A. Leygue, F. Bordeu, J.V. Aguado, E. Cueto, D. Gonzalez, I. Alfaro, A. Ammar and A. Huerta. Parametric PGD based computational vademecum for efficient design, optimization and control. *Archives of Computational Methods in Engineering*, 20/1, 31-59, 2013.

[8] F. Chinesta, A. Leygue, F. Bordeu, J. V. Aguado, E. Cueto, D. Gonzalez, I. Alfaro, A. Ammar, and A. Huerta. PGD-Based Computational Vademecum for Efficient Design, Optimization and Control. *Archives of Computational Methods in Engineering*, 20(1):31-59, 2013.

[9] F. Chinesta, R. Keunings and A. Leygue. The Proper Generalized Decomposition for advanced numerical simulations. *A primer, Springerbriefs, Springer*, 2014.

[10] R.W. Clough and J. Penzien. Dynamics of structures. *Civil engineering series McGraw-Hill*, New York, NY, 1993

[11] S.H. Crandall. The role of damping in vibration theory. *Journal of Sound Vib.*, 11/1, 3-18, 1970.

[12] E. Cueto, D. González, and I. Alfaro. *Proper Generalized Decompositions: An Introduction to Computer Implementation with Matlab*. SpringerBriefs in Applied Sciences and Technology. Springer International Publishing, 2016.

[13] C. Germoso, J.V. Aguado, A. Fraile, E. Alarcon and F. Chinesta. Efficient PGD-based dynamic calculation of non-linear soil behavior. *Comptes Rendus de l'Academie de Sciences*, 344, 24-41, 2016.

[14] David Gonzalez, Elias Cueto, Francisco Chinesta. Real-time direct integration of reduced solid dynamics equations. *International Journal for Numerical Methods in Engineering.* 2014;99(9):633-653.

[15] S. Gregory, M. Tur, E. Nadal, J.V. Aguado, F.J. Fuenmayor and F. Chinesta. Fast simulation of the pantograph-catenary dynamic interaction. *Finite Elements in Analysis and Design*, 129, 1-13, 2017.

[16] M.H. Malik, D. Borzacchiello, F. Chinesta and P. Diez. Inclusion of Frequency Dependent Parameters in Power Transmission Lines Simulation using Harmonic Analysis and Proper Generalized Decomposition. *International Journal of Numerical Modelling: Electronic Networks, Devices and Fields*, In press, https://doi.org/10.1002/jnm.2331.

[17] M.H. Malik, D. Borzacchiello, J.V. Aguado, F. Chinesta. Advanced parametric space-frequency separated representations in structural dynamics: A harmonic-modal hybrid approach. *Comptes Rendus Mècanique*, 346(7): 590-602, 2018.